

# Low-dimensional azimuthal characteristics of suddenly expanding axisymmetric flows

By C. E. TINNEY<sup>1</sup>†, M. N. GLAUSER<sup>1</sup>, E. L. EATON<sup>2</sup>‡  
AND J. A. TAYLOR<sup>2</sup>

<sup>1</sup>Department of Mechanical and Aerospace Engineering, Syracuse University,  
Syracuse, NY 13244, USA

<sup>2</sup>Department of Mechanical and Aeronautical Engineering, Clarkson University,  
Potsdam, NY 13699, USA

(Received 12 November 2004 and in revised form 13 June 2006)

Two rakes of cross-wire probes were used to capture the two-point velocity statistics in a flow through an axisymmetric sudden expansion. The expansion ratio of the facility is 3, and has a constant geometry. Measurements were acquired at a Reynolds number equal to 54 000, based on centreline velocity and inlet pipe diameter. The two-point velocity correlations were obtained along a plane normal to the flow ( $r, \theta$ ), at eleven downstream step-height positions spanning from the recirculating region, through reattachment, and into the redeveloping region of the flow. Measurements were acquired by means of a flying-hot-wire technique to overcome rectification errors near the outer wall of the pipe where flow recirculations were greatest. A mixed application of proper orthogonal (in radius) and Fourier decomposition (in azimuth) was performed at each streamwise location to provide insight into the dynamics of the most energetic modes in all regions of the flow. This multi-point analysis reveals that the flow evolves from the Fourier-azimuthal mode  $m = 2$  (containing the largest amount of turbulent kinetic energy) in the recirculating region, to  $m = 1$  in the reattachment and redeveloping regions of the flow. An eigenvector reconstruction of the kernel, using the most energetic modes from the decomposition, displays the spatial dependence of the Fourier-azimuthal modes and the characteristics that govern the turbulent shear layer and recirculating regions of the flow.

---

## 1. Introduction

Understanding the dynamic behaviour of separated flows is of immense importance for improving and manipulating many practical fluid engineering problems. The axisymmetric sudden expansion is a key canonical separated flow that exhibits this highly complex flow phenomenon. Industrial applications of sudden expansions are seen in the automotive and aerospace industries. In particular, sudden expansions are examined extensively in the propulsion industry because of their similarities to sudden dump combustors. Swirl is introduced at the expansion, and the recirculation region is used as a flame holder. From a scientific standpoint, insightful information about the fundamental behaviours of massively separated flows can be obtained using sudden expansion-type geometries.

† Laboratoire d'Études Aérodynamiques - UMR CNRS 6609, Université de Poitiers, France.

‡ Present address: Ford Motor Company, Dearborn, MI, NY, USA.

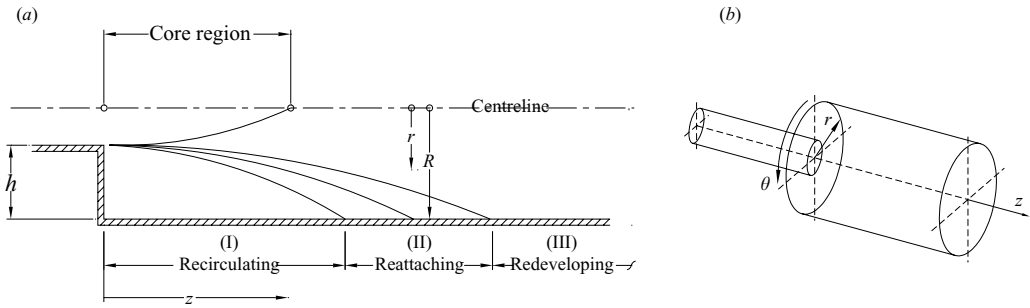


FIGURE 1. (a) A slice in the  $(z, r)$ -plane of the sudden expansion, identifying the predominant regions of the flow: recirculating, reattaching, and redeveloping. (b) Cylindrical coordinate system in the axisymmetric sudden expansion.

Although the flow through an axisymmetric sudden expansion is three-dimensional in nature, most of the attention has been given to the radial ( $r$ ) and streamwise ( $z$ ) plane because of the flow's mean azimuthal invariance. It is in this plane ( $r, z$ ) that there exist three regions of interest: recirculating, reattaching, and redeveloping (figure 1a). As the flow passes over the expansion lip, a free shear layer is formed, thus creating a high-speed side (located near the free-stream flow) and a low-speed side (located near the wall). Eventually the outer shear layer migrates towards the wall, thus impacting its surface and establishing a reattachment region. Rothe & Johnston (1976) defined this reattachment region as the physical location at which the instantaneous velocity was in either forward or reverse flow 50% of the time, and where the Reynolds stresses were found to decay most rapidly.

Early investigations of axisymmetric expansions by Chaturvedi (1963) used Pitot tubes and constant temperature anemometry (CTA) techniques (hot wires) to obtain mean and fluctuating profiles, respectively, and reported a noticeable mutation in the turbulent structures outside the recirculating region near reattachment. Unfortunately, the findings were limited by the unavailability of suitable measuring techniques for high-turbulence-intensity reversing flows, so their results are enigmatic. Bradshaw & Wong (1972) later investigated the simple back-step flow and discovered that the Reynolds stress decay was created by the presence of a strong adverse pressure gradient and the absence of a normal velocity ( $v=0$ ) at the wall, causing large eddies to be torn in two. Furthermore, Eaton & Johnston (1981) identified five parameters that governed the reattachment length: (i) initial boundary layer state, (ii) initial boundary layer thickness, (iii) free-stream turbulence, (iv) pressure gradient, and (v) aspect ratio. The reader is referred to Eaton & Johnston (1981) for a more comprehensive discussion of results using hot-wire, pulsed-wire, laser anemometry and flow visualization techniques.

Cole & Glauser (1998b) illustrated the flow's unsteady behaviour through the axisymmetric sudden expansion using conditional eddy estimation techniques, via multiple channels of simultaneously sampled CTA probes. They reconstructed an instantaneous estimate of the turbulent structure in the  $(r, z)$ -plane based on *a priori* knowledge about the statistical relationship between the core and recirculating regions of the flow (this technique utilized the flying-wire system used in the present study and is described in § 3.1). This involved placing stationary cross-wire probes in the flow's core region where turbulence intensities were moderate, and where there was no reverse flow. In doing so, they were able to properly estimate the flow's highly

unsteady near-wall region, thus concluding that the coherent structures from the near-field shear layer (upstream near the expansion lip) had propagated towards the wall, causing the unsteadiness in the reattachment region. These findings were similar to Johnston (1976), who reported large-scale structures of the order of the step-height convecting through this region.

Additional findings from Cole & Glauser (1998*a*) showed that for an expansion ratio of 3, the turbulent kinetic energy (TKE) was highest between 5 and 8 step-heights downstream from the expansion lip, at  $r/R \approx 0.2$ . This was thought to occur near the core because of the merging of the inner shear layers. Also, the TKE production was observed to reach its maximum within the first four step-heights, while the reattachment length was about 9 step-heights from the expansion lip. These findings were consistent with those of Stokes (1999) and Hussein, Capp & George (1994) in the backward-facing step and the axisymmetric-jet shear layer, respectively.

While these investigations have focused on the  $(r, z)$ -plane of the axisymmetric sudden expansion, a lack of clarity still persists regarding the role of the azimuthal structure on the mean turbulent motions of these flows, especially in the unsteady reattachment region. This paper presents an investigation using multi-point flying-hot-wire measurements with low-dimensional analytical tools in the  $(r, \theta)$ -plane of the axisymmetric sudden expansion to demonstrate the modal behaviour of this wall-bounded flow. This is executed at several streamwise locations ( $z/h = 3$  to 13), covering all three regions of the flow: recirculating, reattaching and redeveloping. The analytical tools comprise a Fourier-azimuthal decomposition of the azimuthal field into azimuthal modes, followed by a decomposition of the radial field using proper orthogonal decomposition (POD). This work complements that of Cole (1996) who applied the one-dimensional POD (in  $r$ ) to the fluctuating velocity field at several streamwise locations in the same facility. Cole (1996) concluded that the first POD mode consistently captured between 35 % and 40 % of the TKE from  $z/h = 2$  to 13, and nearly 50 % of the energy with the addition of the second POD mode. Therefore, these investigations stem from an interest in understanding the importance of the azimuthal structure in this wall-bounded flow, and its characteristics through the recirculating, reattaching and redeveloping regions of the flow.

The outline of this paper is as follows. A brief description of the low-dimensional techniques is given in §2, followed by a description of the experiment, the flying-wire technique, and a discussion of the basic statistical features of the flow through the axisymmetric sudden expansion in §3. Radial and azimuthal correlations are presented and discussed in §4 in a manner fitting to the analytical tools employed. The results of the decomposition are shown in §5 including a discrete modal reconstruction of the kernel to demonstrate the dominant characteristics of this wall-bounded flow. Since the geometry of the axisymmetric sudden expansion is in cylindrical coordinates, the current analysis is expressed using the notation of figure 1(*b*).

## 2. Low-dimensional techniques

As has already been mentioned, the main analytical tools employed in this investigation comprise Fourier-azimuthal and proper orthogonal decomposition. The combination of these techniques is not new, and the interested reader should consult the work of Glauser & George (1987), Citriniti & George (2000), and Ukeiley, Seiner & Ponton (1999) regarding the necessary conditions for employing them. Regarding the Fourier decomposition of axisymmetric turbulent flows (Glauser & George 1987*a*), mean statistical properties from single-point stationary measurements acquired at two

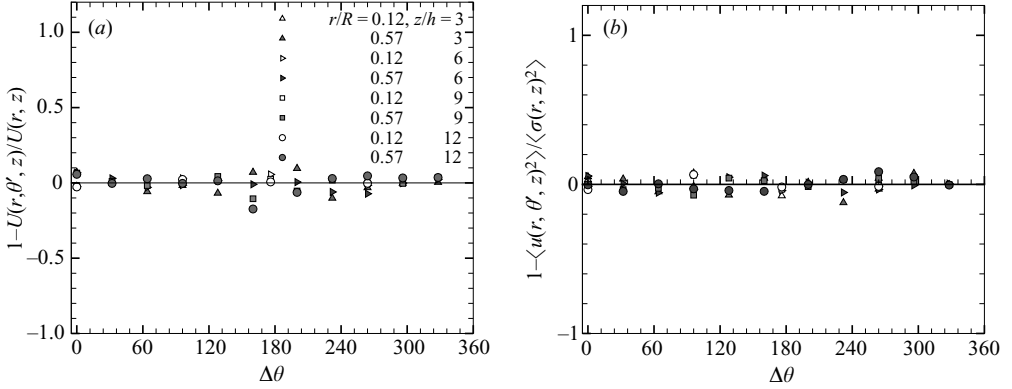


FIGURE 2. The azimuth variation of the streamwise (a) mean velocity (b) Reynolds stress.

different radial locations in the sudden expansion geometry are shown in figure 2 (the data acquisition system and instrumentation are discussed in § 3.2).  $U(r, z)$  and  $\langle \sigma_u(r, z)^2 \rangle$  have been averaged over the azimuth (where  $\theta' = \theta_o + \Delta\theta$ ) to show that the aberration of the streamwise mean and Reynolds stresses is within 10%. Therefore, the Fourier-azimuthal decomposition of the azimuthal spatial correlations is a fitting tool for extracting the most energetic azimuthal modal features of this flow. For the radial direction, Lumley's (1967) POD is most effective.

Some of the more general mathematical properties of the POD are outlined in Aubry *et al.* (1988) and Berkooz, Holmes & Lumley (1993). In short, the POD seeks to maximize the mean-square projection of a candidate event onto a vector field, via the calculus of variations. The kernel used in the maximization is constructed using Hilbert Schmidt's theory of integral equations with symmetric kernels, and the problem results in an integral eigenvalue equation of the Fredholm type:

$$\int_R B_{ij}(r, r', m, z) \phi_j(r', m, z) r' dr' = \lambda(m, z) \phi_i(r, m, z). \quad (2.1)$$

Here the kernel  $B_{ij}(r, r', m, z)$  is the ensemble-averaged, Fourier-transformed ( $\Delta\theta \rightarrow m$ ) two-point velocity cross-correlation tensor  $R_{ij}(r, r', \Delta\theta, z) = \langle u_i(r, \theta, z, t) u_j(r', \theta', z, t) \rangle$ . The technique is optimal in that most of the energy is contained in the first structure alone, and the orthonormal sequence is ordered ( $\lambda^{(n)} \geq \lambda^{(n+1)}$ ). Since the eigenvalues and eigenfunctions are properties of the kernel, they can be utilized to reconstruct it from

$$B_{ij}(r, r', m, z) = \sum_{n=1}^{\infty} \lambda^{(n)}(m, z) \phi_i^{(n)}(r, m, z) \phi_j^{(n)}(r', m, z), \quad (2.2)$$

and an infinite number of eigenfunctions can be used to reconstruct the original instantaneous velocity:

$$\hat{u}_i(r, m, z, t) = \sum_{n=1}^{\infty} \hat{a}_n(m, z, t) \phi_i^{(n)}(r, m, z) \quad (2.3)$$

with

$$\hat{a}_n(m, z, t) = \int_R \hat{u}_i(r, m, z, t) \phi_i^{(n)}(r, m, z) r dr. \quad (2.4)$$

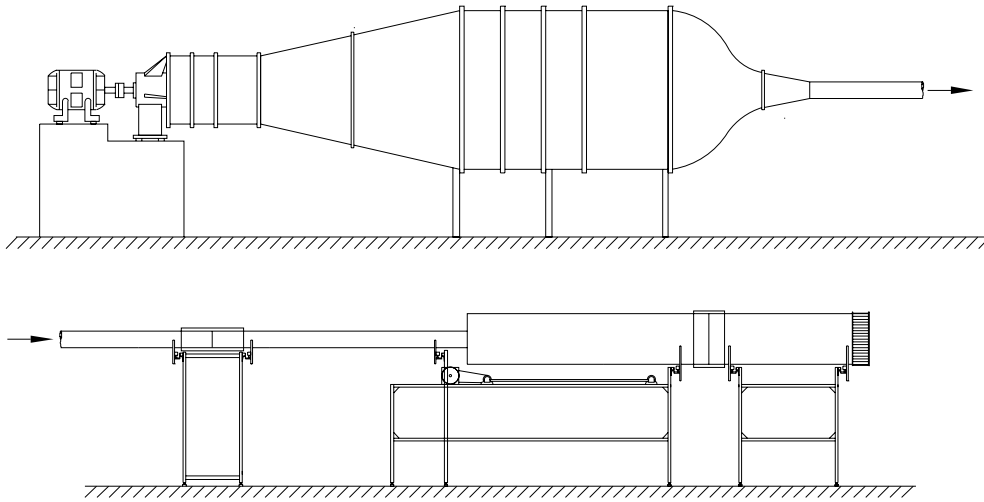


FIGURE 3. Axisymmetric sudden expansion experimental facility.

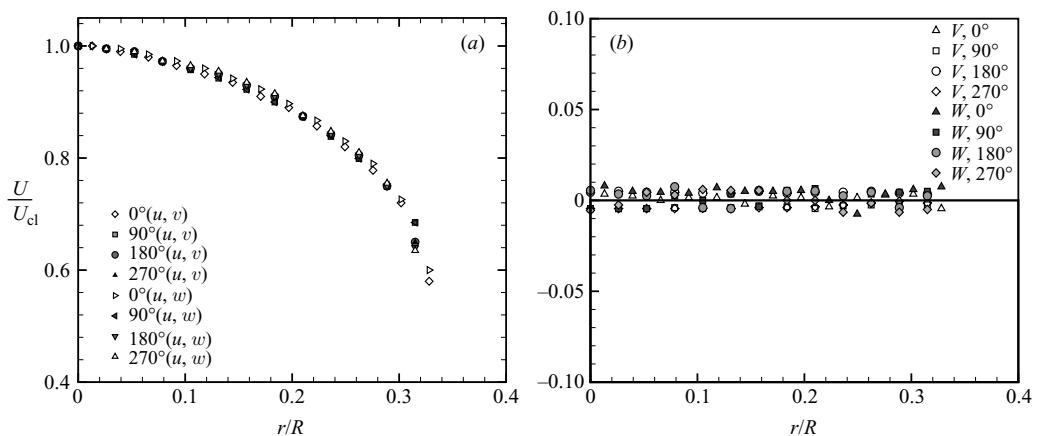


FIGURE 4. Mean velocity profiles at the expansion inlet: (a) streamwise component: (b) radial ( $V/U_{cl}$ ) and azimuthal ( $W/U_{cl}$ ).

### 3. Experiment

The axisymmetric sudden expansion, located in the College of Engineering at Clarkson University, is depicted in figure 3. Details of the tunnel and air supply can be found in Cole & Glauser (1998b), Eaton (1999) and Tinney, Eaton & Glauser (2002a), whereas only the highlights will be discussed here. The test section comprises an expansion ratio of 3 (expanding from a 76 mm diameter pipe to a 228 mm diameter pipe), and is 1.52 m in length. A small slot milled along the bottom surface of the expansion allows a probe sting to be mounted on a flying traversing mechanism (parallel with the axis of the tunnel) located on a bench outside the expansion's test section. The air that is fed to the expansion test section is conditioned by a 76 mm pipe, 3.66 m in length. The length-to-diameter ratio of the pipe (48:1) ensures fully developed flow at the inlet to the expansion test section.

Profile measurements at the inlet to the expansion were acquired using a cross-wire probe positioned along four planes ( $0^\circ, 90^\circ, 180^\circ, 270^\circ$ ), and are shown in figure 4.

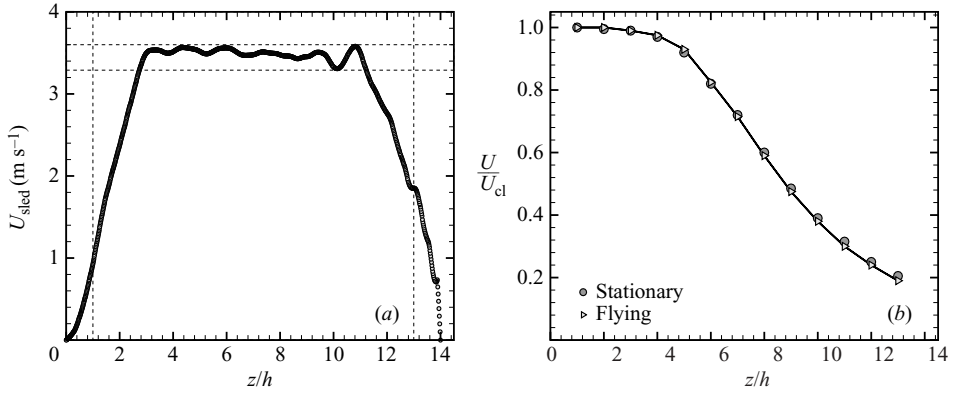


FIGURE 5. (a) Average motion profile of flying-wire traverse using single-wire probe. (b) Comparisons between stationary- and flying-wire probe on the centreline.

Details of the data acquisition system and instrumentation are discussed in §3.2. These profiles were created from an ensemble average of five statistically independent blocks (2048 samples/block) sampled at 100 Hz and are shown in figure 4(a) to collapse extremely well, given the statistical uncertainty of the measurements ( $\approx 3\%$ ). Based on the solution given by Blasius where  $U = 0.99U_{cl}$ , the average boundary layer at the inlet was found to be 7.06 mm, or  $0.093D$  thick.  $D$  for this calculation is the diameter (76 mm) of the smaller pipe at the inlet to the expansion; and the inlet mass flow rate, expressed as a function of the centreline velocity, was calculated to be  $4.7 \times 10^{-3}U_{cl}$ . Likewise, the mean radial ( $V/U_{cl}$ ) and azimuthal ( $W/U_{cl}$ ) velocities at the inlet are shown in figure 4(b) and are essentially zero. This indicates that there is no appreciable swirl at the inlet to the sudden expansion. Measurements were conducted at a Reynolds number of 54 000, based on centreline velocity ( $U_{cl} = 10.35 \text{ m s}^{-1}$ ) and inlet pipe diameter.

### 3.1. Flying wire

Due to the directional ambiguity of hot-wire anemometry, the flying-wire technique was used to capture the two-point statistics in regions where reverse flow and hot-wire rectification errors were likely, as was commonly found along the outer wall regions of the flow. This technique has been well documented (Watmuff, Perry & Chong 1983; Panchapakesan & Lumley 1993). Its advantage is the ability to improve the linearity of the probe's response by imposing a large bias velocity on the probe's sensing wire, thereby reducing the cone-angle between the probe's axis and the oncoming velocity vector, and ultimately improving the accuracy of the measurements.

In the present study, a stepper motor accelerated and decelerated a sled (that the probe rake was attached to) to a prerecorded impulse velocity near  $3.5 \text{ m s}^{-1}$  between  $z/h = 14$  and  $z/h \approx 0$ . During each sled pass, the position of the stepper motor was recorded simultaneously with the CTA's output so that the position of the probe was known during its acquisition. Special attention was given to the alignment of the sled traverse with respect to the tunnel's axis, so that the vertex of the probe rake was located in the centre of the tunnel during its entire streamwise displacement. Furthermore, the mean impulse velocity of the sled, shown in figure 5(a), was acquired using a single-wire probe averaged over 1024 runs, without flow through the tunnel. This was later subtracted from measurements taken when the tunnel was turned on. Flying-wire measurements were then repeated with the tunnel turned on and were

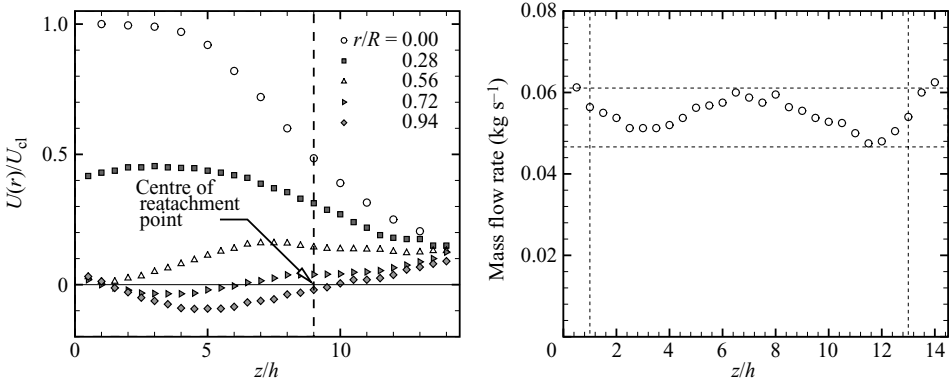


FIGURE 6. (a) Mean streamwise velocity profiles, where  $U_{cl} = 10.35 \text{ m s}^{-1}$ . (b) Mass flow rate calculated with the single cross-wire data.

compared with stationary measurements under the same flow conditions in an attempt to reconcile any differences between the two techniques. Excellent accordance can be seen between the two data-sets shown in figure 5(b), despite small variations in the averaged motion profile of the sled. Mean streamwise velocity profiles ( $U/U_{cl}$ ) using this flying-wire technique are shown in figure 6(a), demonstrating the effectiveness of this technique in sensing the outer wall regions of the flow where flow reversals are common.

Due to the physical nature of wall-bounded flows, the principle of mass conservation was calculated using the measurements from figure 6(b) and a trapezoidal substitution for

$$\dot{m} = 2\pi\rho \int_0^R U(r)r \, dr. \quad (3.1)$$

The results are shown in figure 6(b). In general, the mass flow rate is slightly lower before and after the reattachment region (near  $z/h = 8$  and 9), presumably a result of the synthesis of small statistical errors in the measurements and numerical integration error. Had these errors been a result of flow leakage, one would expect to see a lower mass flux at the downstream location. Cole (1996) investigated this phenomenon in more detail and found many qualitative similarities with other investigators.

### 3.2. Data acquisition and instrumentation

The cross-wire measurements incorporated sixteen differential channels of thermal anemometry, each sampled at a frequency of 2 kHz and low-pass filtered at 820 Hz. The eight probes comprised custom built *Auspex* cross-wires, with tungsten wire sensing lengths ( $l_w$ ) of 1.0 mm and diameters of 5  $\mu\text{m}$  (aspect ratio of 200). Given the radial and streamwise variations of the mean velocities, the corner frequency  $f_c = U(r, z)/2l_w$  ranged between 5.2 kHz and 1.2 kHz for the flying-wire measurements, and between 4.1 kHz and 420 Hz for any stationary measurements at the Reynolds number studied.

Data acquisition was accomplished using 16-bit resolution *IOTech* analog-to-digital converters with simultaneous sample and hold. Quantization errors for these instruments are on the order of  $3 \times 10^{-4} \text{ V}$  for a  $\pm 10 \text{ V}$  bipolar range. The calibration procedure for the cross-wires, described in Cole & Glauser (1998b) and Eaton (1999), used an expression relating the free-stream velocity  $U_o$  to the effective velocity  $U_{\text{eff}}$  (seen by the probe), as suggested by Hinze (1975).

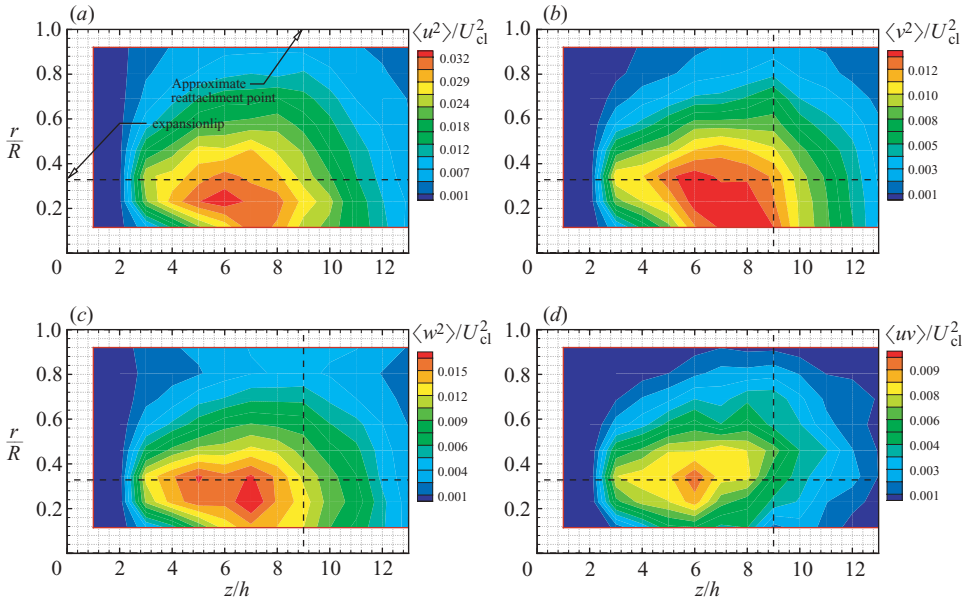


FIGURE 7. The Reynolds stresses.

### 3.3. Reynolds stresses

Figure 7 shows the normal and shear stress profiles obtained from 450 statistically independent sled passes using a single radial rake of cross-wire probes (eight probes) and the flying-wire technique. The maximum values of  $\langle u^2 \rangle$  are shown to comprise the greatest portion of turbulent energy, while  $\langle v^2 \rangle$  and  $\langle w^2 \rangle$  are maximally similar. All of them peak near  $z/h = 7$  before the reattachment point, and fall rapidly (nearly half of their energy is lost) by  $z/h = 10$ . In general these Reynolds stresses demonstrate similar behaviours (in magnitude) to those of Bradshaw & Wong (1972) and Castro & Haque (1987). The streamwise/azimuthal shear stresses  $\langle uv \rangle$  are not shown, as they are insignificant in value.

What is striking about these normal stresses is that until the collapse of the potential core, the location where the turbulent energy peaks is closer to the central regions of the flow (towards  $r/R = 0$ ), rather than the expansion lip line. Gould, Stevenson & Thompson (1990) and Cole & Glauser (1998a) demonstrated nearly identical features, despite differences in the inlet conditions. Though the turbulence model of Gould *et al.* (1990) over-predicted the shear stress values (in some instances), the divergence of the shear layer towards the potential core before its collapse was evident. This is surprising considering the profiles of Castro & Haque (1987), who attributed this augmentation at the shear layer centre-line to the mean streamline curvature, a known phenomenon by which a slightly lower pressure in the recirculating region forces the mean shear layer to curve more rapidly towards the wall than in other free shear flows (i.e. the behaviour of the axisymmetric jet would be the most appropriate comparison to the current study).

Castro & Haque (1987) showed that the normal stresses, as well as the vorticity thickness, were typically larger in the early part of the flow when compared to the planar turbulent mixing layer. Their findings also demonstrated a dominance of the turbulent spanwise energy relative to the normal energy in the reattachment region. This is in correspondence with the current stress profiles (figure 7) which illustrate



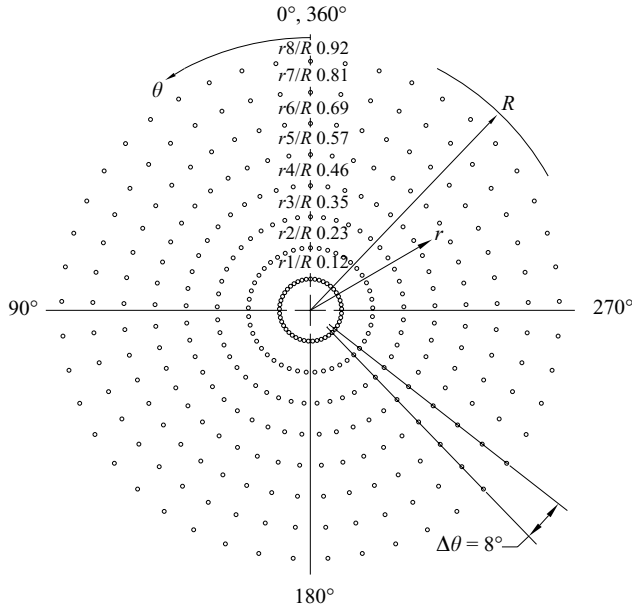


FIGURE 8. Grid density of 8 radial and 45 azimuthal locations for capturing the two-point statistics.

an increase in the azimuthal stresses near the wall regions of the flow, whereas the radial stresses continue to decay due to the wall's impermeability. However, in the axisymmetric sudden expansion, the collapse of the potential core (specifically around  $z/h = 5$ ) reduces the statistical features along the centreline, thus preventing a linearly self-similar solution to the profiles, unlike the investigations of Castro & Haque (1987). Therefore, the range over which a direct comparison could be made between the axisymmetric jet and the current study is limited to a region that does not include many of the features of the flow that are of interest, specifically the reattachment region around  $z/h = 9$ .

The stress profiles shown here comprise perhaps one of several identifiable differences among axisymmetric sudden expansion flows, axisymmetric jets, and the planar backstep/mixing layer studies. Though the axisymmetric sudden expansion possesses characteristic features of the axisymmetric jet (a potential core region) and of the planar backstep flow (streamline curvature), the flow through the axisymmetric sudden expansion produces a turbulence structure that is quite unique, where self-similarity is concerned. We will revisit this discussion in §5.

#### 4. Multi-point cross-wire measurements and the two-point statistics

Multi-point measurements of the azimuthal spatial field were acquired with a probe stinging consisting of two radial rakes of cross-wire probes mounted on the traverse sled, which differs from the rake used in §3. One radial rake was fixed while the other rake had the freedom to pivot between  $0^\circ$  and  $180^\circ$ , relative to the other rake. Following the suggestions of Glauser & George (1992), the mean azimuthal invariance of this flow was considered in the measurement procedure, thus the two-point measurements were performed between  $0^\circ$  and  $180^\circ$ . In doing so, a grid density of 360 total points can be constructed by measuring only half of these points. This grid, shown in figure 8,

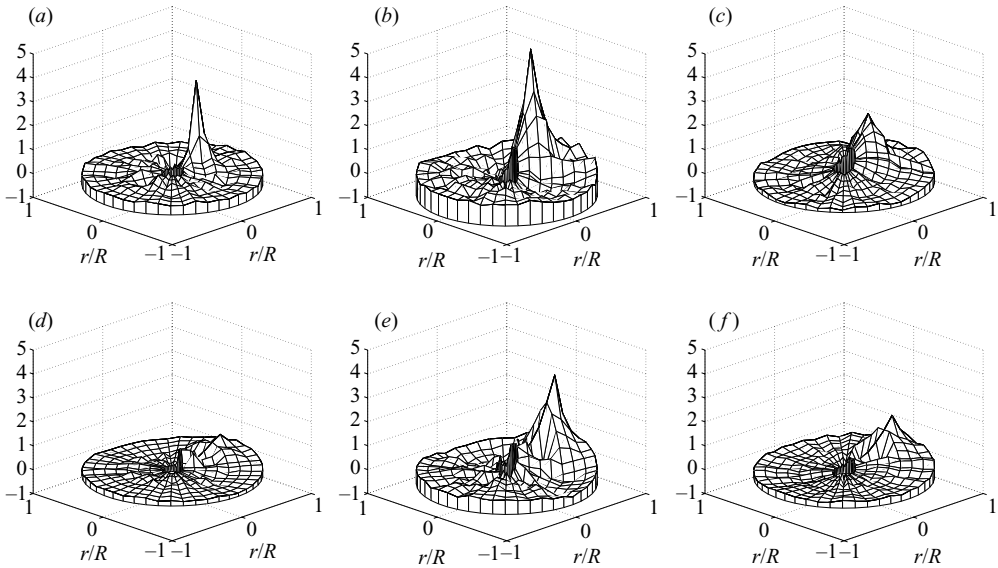


FIGURE 9. The cross correlation  $R_{uu}(r, r', \Delta\theta, z)$ : (a)  $R_{uu}(0.35, r', \Delta\theta, 3)$ , (b)  $R_{uu}(0.35, r', \Delta\theta, 6)$ , (c)  $R_{uu}(0.35, r', \Delta\theta, 12)$ , (d)  $R_{uu}(0.69, r', \Delta\theta, 3)$ , (e)  $R_{uu}(0.69, r', \Delta\theta, 6)$ , (f)  $R_{uu}(0.69, r', \Delta\theta, 12)$ .

identifies the 8 radial ( $\Delta r/R = 0.115$ ) and 45 azimuthal ( $\Delta\theta = 8^\circ$ ) locations used to create the kernel in (2.1). The cross-wires were oriented to measure the velocity's streamwise  $u$  and radial  $v$  components from which normal and shear Reynolds stress terms ( $uu$ ,  $uv$ ,  $vu$  and  $vv$ ) are calculated. For statistical convergence, each two-point measurement comprised 450 statistically independent sled passes, whereby 2048 samples were acquired as the cross-wires were propelled down the length of the tunnel. Based on the Reynolds stress values shown in § 3.3, the percent variance from the mean, using  $\epsilon = \sigma_u(U\sqrt{N})^{-1}$  and  $N = 450$ , was less than 1% in the core and less than 5% at the outer wall.

#### 4.1. Correlations

Several of the correlations were selected to provide the reader with a general picture of the statistical characteristics of the turbulent motions of this flow. In figure 9, the radial and azimuthal characteristics of the correlation function  $R_{uu}(r, r', \Delta\theta, z)$  are illustrated by fixing  $r$  and  $\theta_0$ , and changing  $r'$  and  $\theta'$ . This is shown at three streamwise positions in the flow:  $z/D = 3, 6, 12$ .

In figure 9(a), the correlation tensor  $R_{uu}(0.35, r', \Delta\theta, 3)$  clearly illustrates the initial development of shedding events from the expansion's lip. Given the slow roll-off of  $R_{uu}(0.35, r', \Delta\theta, 3)$ , which is near the centre of the shear layer and close to the lip where one would expect to find a large amount of energy in the higher azimuthal modes (if it existed), it is clear that the dominant length scales in the flow are sufficiently large. Thus, any scales which may have been aliased because of the spatial distances between probes have had a negligible effect on the results. The fact that the topography of the correlation at  $r/R = 0.69$  in figure 9(d) lacks any significant features suggests a relatively dead zone in the flow. Subsequently, figures 9(b) and 9(e) show a growth of the coherent structure at both radial positions. Closer observation indicates that the peak is taller and narrower at  $r/R = 0.35$  than at  $r/R = 0.69$ ; however the azimuthal length scale is shown to encompass a much broader area at the higher

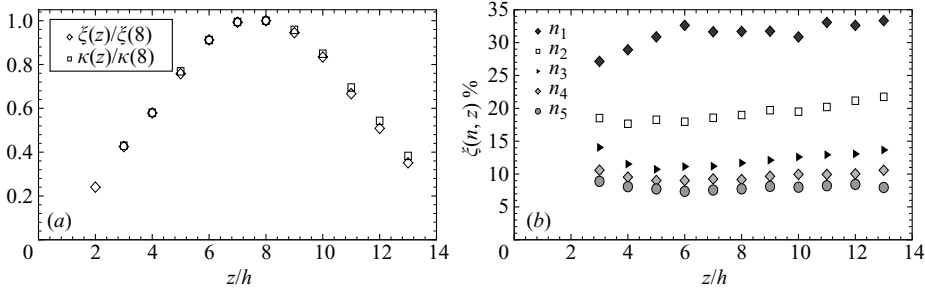


FIGURE 10. (a) Total eigenspectra energy  $\zeta(z)$  and the TKE  $\kappa(z)$ . (b) Local contribution (%) of POD modes 1 to 5 to total energy.

radial position. There were similar findings at  $z/h=9$  (not shown), characterizing a radial and axial growth of the turbulent structure. In the redeveloping region of the flow at  $z/h=12$  (figure 9c, f), a decrease of the radial correlation results in the broadening of the azimuthal length scales.

## 5. Results of the modal analysis

A comparison of a full summation of the eigenmodes

$$\zeta(z) = \sum_n \sum_m \lambda^{(n)}(m, z), \quad (5.1)$$

with the total TKE is shown in figure 10(a), thus demonstrating the axial location (around  $z/h=8$ ) where the turbulence activity is greatest. These results have qualitative similarities to those of Cole & Glauser (1998a) and show a consistency between direct measurements of the TKE and the solutions from the decomposition.

The total energy of the first 5 POD modes

$$\xi(n, z) = \frac{\sum_m \lambda^{(n)}(m, z)}{\zeta(z)}, \quad (5.2)$$

is shown in figure 10(b), and it is similar to other applications of these techniques where a large percentage of the local energy ( $\sim 30\%$ ) is captured in the first radial POD mode alone. With the first two POD modes combined, nearly 50% of the energy is contained, and so on. A slight increase in the relative energy contained in the first (largest) POD eigenvalue implies that the development of the radial structure becomes more coherent as it convects downstream from the expansion lip. In subsequent figures, only the first few POD modes will be used, as they have been shown to comprise sufficient amount of the total turbulent energy.

### 5.1. Eigenvalue distribution

The eigenvalue distributions are shown in figure 11, normalized by (5.1). Upstream towards the expansion lip ( $z/h=3$  in figure 11a), the distribution of the Fourier-azimuthal energy is fairly broadband, in contrast to a coalescence of energy in the lower azimuthal modes shown in successive figures. The fully developed profile at the inlet to the expansion is responsible for this as Cole (1996) has shown that the turbulent spectral densities are broad in this region of the flow. As the flow evolves downstream, the integral scales increase, and the energy becomes less broad and

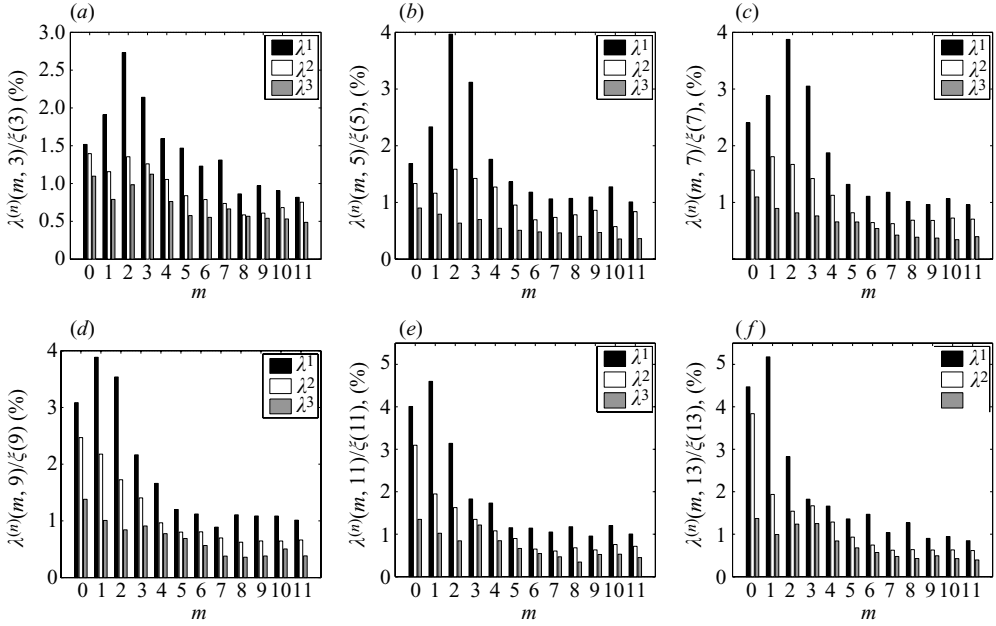


FIGURE 11. Eigenvalue distribution of the first three POD modes and azimuthal modes 0 to 11 at (a)  $z/h = 3$ , (b)  $z/h = 5$ , (c)  $z/h = 7$ , (d)  $z/h = 9$ , (e)  $z/h = 11$ , (f)  $z/h = 13$ .

more low-dimensional in azimuth. No dramatic change in the eigenspectra was found beyond azimuthal mode  $m = 6$  for all step-heights, with a preponderance of energy in the first few azimuthal modes, primarily  $m = 0, 1, 2$  and  $3$ . This suggests a small level of aliasing in the azimuthal decomposition, and that the azimuthal grid's resolution was satisfactory for resolving the spatial modes of this flow.

The most striking feature of the eigenspectra is the pronounced modal switching, demonstrated in figure 11(d, e), that occurs in the reattaching region of the flow. While the azimuthal mode 2 dominates the recirculating zone of the flow, it succumbs to the helical mode 1 after reattachment and into the initial stages of the redeveloping regions of the flow. This differs drastically from the azimuthal modal behaviour of the axisymmetric jet (Glauser & George 1987; Citriniti & George 2000) which has demonstrated a dominance in the first symmetric  $m = 0$  mode, followed by higher modes 4, 5 and 6. Bradshaw & Wong (1972) observed the creation of a ‘unique’ structure at reattachment caused by a change in the shear layer’s mass flow. Despite little change in the velocity gradient ( $\partial U / \partial r$ ), they simply proposed that the impermeability of the wall caused the absence of a normal velocity component ( $v = 0$ ), resulting in a rapid decay of the Reynolds shear stress. The decay of the shear stress terms has been observed in many reattaching flows (Chandrsuda & Bradshaw 1981; Castro & Haque 1987; Eaton & Johnston 1981), regardless of large differences in the initial conditions, and this decay has been generally attributed to the mean streamline curvature.

### 5.2. Modal reconstruction of the kernel

The eigenvectors are now used to reconstruct the kernel  $B_{ij}$

$$B_{ij}^{(N)}(r, m, z) = \sum_{n=1}^2 \lambda^{(n)}(m, z) \phi_i^{(n)}(r, m, z) \phi_j^{(n)*}(r, m, z), \quad (5.3)$$

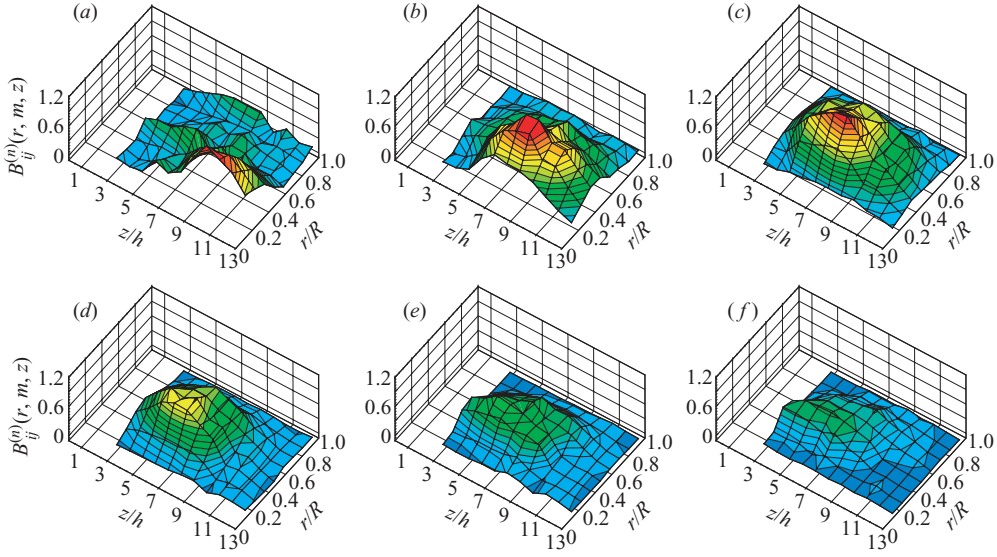


FIGURE 12. The eigenvector reconstruction of  $B_{ij}$  with POD modes for several Fourier-azimuthal modes: (a)  $B_{11}^{1+2}(r, 0, z)$ , (b)  $B_{11}^{1+2}(r, 1, z)$ , (c)  $B_{11}^{1+2}(r, 2, z)$ , (d)  $B_{11}^{1+2}(r, 3, z)$ , (e)  $B_{11}^{1+2}(r, 4, z)$ , (f)  $B_{11}^{1+2}(r, 5, z)$ .

with  $r = r'$  for various azimuthal mode numbers. Only the first two POD modes ( $\sim 50\%$  of the turbulent energy) will be used in the reconstructions, since additional POD modes were found to have little effect on the principle turbulent features. The results are presented in figure 12.

For the axial component of velocity, it is clear that the axisymmetric mode (figure 12a) dominates the shape of the flow structure leading towards reattachment and through the recirculating regions of the flow. Though the next few modes have been shown to possess more turbulent energy (overall), they are clearly confined to the shear layer regions and contribute very little to the regions where the axisymmetric mode is shown to dominate. Reconstructions of the higher Fourier-azimuthal modes  $m = 4$  and  $m = 5$  show the streamline curvature of the flow. Therefore, the adverse pressure effects due to the expansion wall only affect the higher modes. Furthermore, the energy of the higher modes decays rapidly as they approach the outer wall, leaving the outer recirculating region dominated by an axisymmetric structure, once more. The decay in energy of all other higher modes ( $m > 5$ ) after reattachment is like the behaviour of the  $m = 5$  eigenvector reconstruction shown in figure 12(f).

## 6. Conclusion

The decomposition of the streamwise and radial components of the fluctuating velocity field of the flow through an axisymmetric sudden expansion was investigated using proper orthogonal and Fourier decomposition in radius and azimuth, respectively. The decomposition was performed along slices of the  $(r, \theta)$ -plane, at several streamwise positions, starting from the recirculating region ( $z/h = 3$  to  $7$ ), through the reattachment region ( $z/h = 7$  to  $9$ ), and into the beginning stages of the redeveloping region ( $z/h = 9$  to  $13$ ) of this flow. The experimental method employed a flying-wire technique which was shown to effectively capture the multi-point statistics

using cross-wire CTA tools in a flow characterized by regions of high turbulence intensities and flow recirculations.

The eigenvalues from the decomposition have brought out the dominance of the Fourier-azimuthal and POD modes that govern a moderate to large percentage of this highly unsteady wall-bounded flow. The results of the POD showed that approximately 30% and 20% of the total energy was contained in the first and second modes, respectively, through all streamwise positions studied. The Fourier-decomposition of the azimuthal structure indicated a noticeable shift in the energy near reattachment, from a flow dominated by an  $m = 2$  mode to one dominated by an  $m = 1$  mode. A reconstruction of the axial component of the eigenvectors showed that the reattachment and recirculating regions near the outer wall were strictly dominated by an axisymmetric structure, whereas the shear layer regions comprised a contribution from the helical and azimuthal modes 2 and 3. Higher modes 4 and 5 were found in the low-speed regions near the outer wall of the shear layer and were clearly shown to follow the streamline curvature of the flow towards the wall at reattachment where they decayed drastically in energy before impinging on the wall.

#### REFERENCES

- AUBRY, N., HOLMES, P., LUMLEY, J. & STONE, E. 1988 The dynamics of coherent structure in the wall region of a turbulent boundary layer. *J. Fluid Mech.* **192**, 115–173.
- BERKOOZ, G., HOLMES, P. & LUMLEY, J. L. 1993 The Proper Orthogonal Decomposition in the analysis of turbulent flows. *Annu. Rev. Fluid Mech.* **25**, 539–575.
- BRADSHAW, P. & WONG, F. Y. F. 1972 The reattachment and relaxation of a turbulent shear layer. *J. Fluid Mech.* **52**, 113–135.
- CASTRO, I. P. & HAQUE, A. 1987 The structure of a turbulent shear layer bounding a separation region. *J. Fluid Mech.* **179**, 439–468.
- CHANDRSUDA, C. & BRADSHAW, P. 1981 Turbulence structure of a reattaching mixing layer. *J. Fluid Mech.* **110**, 171–194.
- CHATURVEDI, M. C. 1963 Flow characteristics of axisymmetric sudden expansions. *Proc. ASCE, J. Hydraulics Div.* **89**, 61–92.
- CITRINITI, J. H. & GEORGE, W. K. 2000 Reconstruction of the global velocity field in the axisymmetric mixing layer utilizing the proper orthogonal decomposition. *J. Fluid Mech.* **418**, 137–166.
- COLE, D. R. 1996 Utilizing a flying hot-wire system to study the flow in an axisymmetric sudden expansion. PhD Dissertation, Rep. MAE-328, Clarkson University, Potsdam, NY.
- COLE, D. R. & GLAUSER, M. N. 1998a Flying hot-wire measurements in an axisymmetric sudden expansion. *Expl. Therm. Fluid Sci.* **18**, 150–167.
- COLE, D. R. & GLAUSER, M. N. 1998b Applications of stochastic estimation in the axisymmetric sudden expansion. *Phys. Fluids* **10**, 2941–2949.
- EATON, E. L. 1999 An examination of the azimuthal variation using multi-point measurements in the axisymmetric sudden expansion. PhD Dissertation, Rep. MAE-337, Clarkson University, Potsdam, NY.
- EATON, J. K. & JOHNSTON, J. P. 1981 A review of research on subsonic turbulent flow reattachment. *AIAA J.* **19**, 1093–1100.
- GLAUSER, M. N. & GEORGE, W. K. 1987 Orthogonal decomposition of the axisymmetric jet mixing layer including azimuthal dependence. In *Advances in Turbulence* (ed. G. Comte-Bellot & J. Mathieu), pp. 357–366. Springer.
- GLAUSER, M. N. & GEORGE, W. K. 1992 Application of multipoint measurements for flow characterization. *Expl. Therm. Fluid Sci.* **11**, 617–632.
- GOULD, R. D., STEVENSON, W. H. & THOMPSON, H. D. 1990 Investigation of turbulent transport in an axisymmetric sudden expansion. *AIAA J.* **28**, 276–283.
- HUSSEIN, H. J., CAPP, S. P. & GEORGE, W. K. 1994 Velocity measurements in a high Reynolds-number, momentum-conserving, axisymmetric turbulent jet. *J. Fluid Mech.* **258**, 31–75.
- HINZE, J. O. 1975 *Turbulence*. 2nd edn. McGraw Hill.

- JOHNSTON, J. P. 1976 Internal flows. In *Turbulence* (ed. P. Bradshaw) Springer.
- LUMLEY, J. L. 1967 The structure of inhomogenous turbulent flows. In *Atmospheric Turbulence and Radio Wave Propagation*. Nauka, Moscow.
- PANCHAPAKESAN, N. R. & LUMLEY, J. L. 1993 Turbulence measurements in axisymmetric jets of air and helium. Part 1. Air jet. *J. Fluid Mech.* **246**, 197–223.
- ROTHER, P. H. & JOHNSTON, J. P. 1976 Free shear layer behavior in rotating systems. *Trans. ASME: J. Fluids Engng* **101**, 117–120.
- STOKES, S. D. 1999 Single and multi-point measurement techniques used in the study of separated flows. PhD Dissertation, Rep. MAE-340, Clarkson University, Potsdam, NY.
- TINNEY, C. E., EATON, E. L. & GLAUSER, M. N. 2002a Multi-point measurements in an axisymmetric sudden expansion. *Proceed 5th Intl Symp. on Engineering Turbulence Modelling and Measurements* (ed. W. Rodi & N. Fueyo) Mallorca, Spain, pp. 485–494.
- UKEILEY, L., SEINER, J. & PONTON, M. 1999 Azimuthal structure of an axisymmetric jet mixing layer. *ASME FEDSM99-7252*, July.
- WATMUFF, J. H., PERRY, A. E. & CHONG, M. S. 1983 A flying hotwire system. *Exps. Fluids* **1**, 67–71.